ISSN 0280–5316
ISRN LUTFD2/TFRT--5666--SE

System Identification applied to Cardiac Activation

Susana Santos

Department of Automatic Control
Lund Institute of Technology
April 2001

Department of Automatic Control
Lund Institute of Technology
Box 118
SE-221 00 Lund Sweden

Document name
MASTER THESIS

Date of issue
April 2001

Document Number
ISRN LUTFD2/TFRT—5666--SE

Author(s)
Susana Santos

Supervisor
Enrique Baeyens, Univ. of Vallodolid, Spain
Rolf Johansson, LTH

Sponsoring organization

Title and subtitle
System Identification applied to Cardiac Activation
(Systemidentifiering av Kardiell Aktivering)

Abstract
Clarifying the mechanisms maintaining atrial activity during atrial fibrillation (AF), still remains as a relevant topic. The purpose of this master thesis is to apply correlation analysis and system identification methods to study spatial and temporal propagation of atrial activation along coronary sinus (situated in the posterior left part of the heart, in the groove between left atrium and left ventricle) during paroxysmal atrial fibrillation (PAF) using data recorded catheter from 7 different patients. Furthermore, interatrial mechanisms of impulse conduction cam be derived due to the position of coronary sinus. This study demonstrated consistency in electrical activity propagation during atrial fibrillation along coronary sinus in five patients out of six included. Nevertheless, direction and speed of propagation resulted dependent on the patient. The method was tried out during sinus rhythm (SR) obtaining the expected high consistency in propagation direction and speed which represented an interesting reference point to compare with atrial fibrillation results. Furthermore, linear relation among endocardial electrograms from coronary sinus and time invariant systems have been presented by computing simple linear models based on least squares method.
Secondly, an impulse response method has been applied to reproduce atrial activations during atrial fibrillaton and during sinus rhythm in ten endocardial electrograms from coronary sinus simultaneously. In this case, there is no need of measuring the input which is considered to be an impulse generated in the sinus node. This method was only useful in local prediction of atrial activations but not for prediction in the long term.
Finally, Subspace Model Identification (SMI) methods have been applied to show an input-output relation among signals from inside the heart (endocardial electrograms from coronary sinus) and signals from outside the heart (V1 Surface-ECG).

Keywords

Classification system and/or index terms (if any)

Supplementary bibliographical information

ISSN and key title
0280-5316

ISBN

Language
English

Number of pages
46

Recipient's notes

Security classification

Contents

Acknowledgments 7

1. Introduction 9
- 1.1 Heart description 9
- 1.2 The circulatory system 9
- 1.3 The conduction system, propagation of the electrical impulse 10
- 1.4 Surface Electrocardiograms (Surface-ECG) 11
- 1.5 Arrhythmias: Atrial Fibrillation (AF) 11
- 1.6 Cardiac Catheterization 13

2. Previous studies and motivation 14

3. The objectives of the present study 16

4. Materials and methods: Catheterization 17

5. Reproduce atrial activations applying an impulse response method 19
- 5.1 Objective 19
- 5.2 Signal analysis 19
- 5.3 System identification method 19
- 5.4 Validation 21
- 5.5 Results 22
- 5.6 Conclusions 24

6. Subspace Model Identification (SMI) methods applied to endocardial and surface ECG 27
- 6.1 Objective 27
- 6.2 Signal Analysis 27
- 6.3 PO-MOESP Algorithm 27
- 6.4 Validation 30
- 6.5 Results 30
- 6.6 Conclusions 31

7. Spatial and temporal propagation of atrial activity during AF and SR 35
- 7.1 Objective 35
- 7.2 Signal Analysis 35
- 7.3 Correlation analysis on complete signals 35
- 7.4 Calculating the excitation direction and velocity component 36
- 7.5 Substitution of ventricle response by a linear interpolation in all coronary sinus catheter signals 37
- 7.6 Correlation analysis on signals with substituted ventricle response 37
- 7.7 System identification applied to verify previous results . . . 39
- 7.8 Model Validation 40
- 7.9 Results 40
- 7.10 Discussion 43
- 7.11 Conclusions 47

8. Final Conclusions 48

9. Bibliography 49

Acknowledgments

I want to express my sincere gratitude to everyone who has helped and supported me during this work. I want to send special thanks to:

- Prof. Rolf Johansson, my advisor, for trusting and supporting me during all the work with enthusiasm and precious supervision.
- Prof. S. Bertil Olsson, for sharing his knowledge in the medical field with me and giving me the opportunity to research in an exciting subject.
- Jonas Carlson and Eva Hertervig, for patiently introducing me in the subject and helping me with the engineering and medical problems respectively.
- All the people at the Automatic Control Department for making me feel at home during these six months in Sweden.
- All the people at the Cardiology Department for bearing my short knowledge in the medical field and for helping me with interpretations and ideas to go on with my work.
- Last but not least, Prof. Enrique Baeyens, my Spanish advisor, who introduced me in the subject and arouse my interest in the fascinating world of control theory.

1. Introduction

1.1 Heart description

The heart works as a pump that pushes blood to the organs, tissues and cells of the body. Blood delivers oxygen and nutrients to every cell and removes the carbon dioxide and waste products made by those cells. Blood is carried from the heart to the rest of your body through a complex network of arteries, arterioles and capillaries and it is returned to the heart through venules and veins.

The heart has four chambers. See Fig. 1.1. The upper chambers are left and right atria and the lower ones are called left and right ventricles. A wall of muscle called the septum divides the heart in two parts: the low pressure right atrium and ventricle occupy the anterior portion of the heart and the higher pressure left atrium and ventricle lie posteriorly.

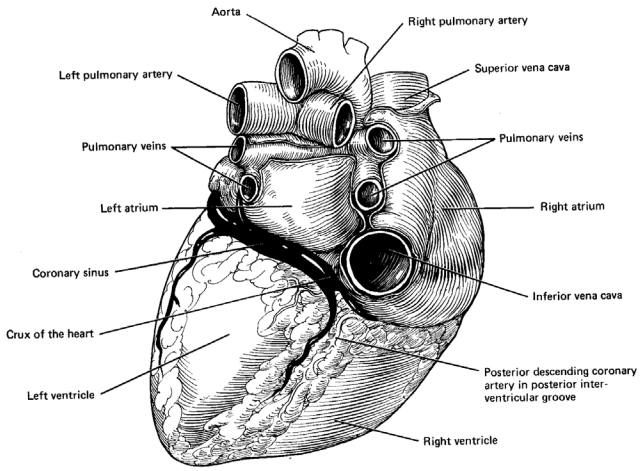

Figure 1.1 The heart viewed from bellow and behind.

1.2 The circulatory system

The one-way circulatory system carries blood to all parts of the body. The right atrium receives oxygen-poor blood from the head and upper parts of the body through the superior vena cava and from the lower parts of the body through the inferior vena cava. See Fig. 1.2. Also, it receives oxygen-poor blood from the heart itself through the *coronary sinus*, in the atrioventricle groove. This used-blood is then pushed to the right ventricle through the tricuspid valve. Afterwards, the blood is pumped to the lungs through the pulmonary valve to the pulmonary arteries, providing blood to both lungs. Inside the lungs, carbon dioxide is removed and oxygen added, thus, oxygen-rich blood returns through the pulmonary veins into the left atrium. This chamber, pumps the oxygen-rich blood into the left ventricle

through the mitral valve. Left ventricle is the most important chamber because it pumps through the aortic valve into the aorta artery to the rest of the body.

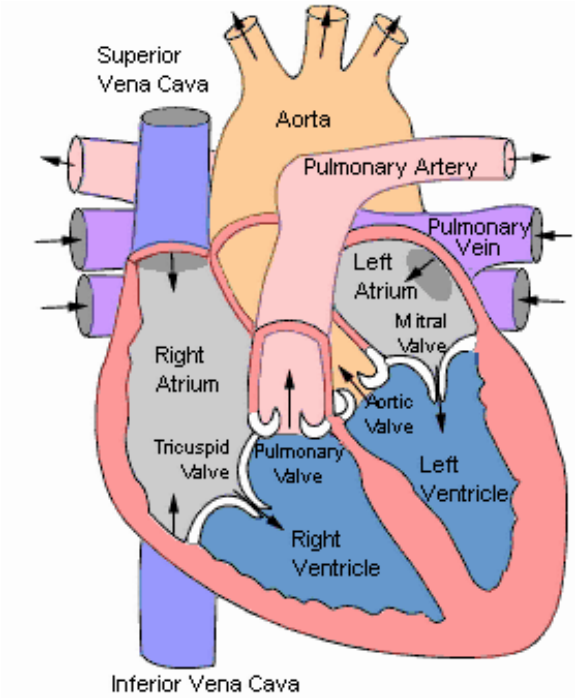

Figure 1.2 The circulatory system.

1.3 The conduction system, propagation of the electrical impulse

Electrical impulses from the myocardium cause the heart to contract, electrical events precede mechanical events. The cardiac cycle starts with the formation of an impulse in the sinoatrial (SA) node, located at the top of the rigth atrium near the superior vena caval orifice, as shown in Fig. 1.3. The sinus node is called the 'natural pacemaker' of the heart. When the sinus node sends out an electrical signal, it causes the atrial contraction. This contraction pushes blood through the tricuspid and mitral valves from the atrium to the resting ventricles, generating the atrial systolic activity. The impulse spreads by several internodal pathways through both atria. When it reaches the atrioventricular (AV) node, near the tricuspid valve, the cells of the bundle of His are activated and the impulse spreads by the Purkinje fibers to activate the ventricles. This causes the ventricular mechanical contraction, generating the ventricular systolic activity. Blood will be pushed through the pulmonary and aortic valves from ventricles to the lungs and to all the body. After atrial and ventricular systole, diastole of the heart starts, ventricles relax and the pulmonary and aortic valves close. Low pressure in the ventricles causes the tricuspid and mitral valves to open, and the cycle begins again.

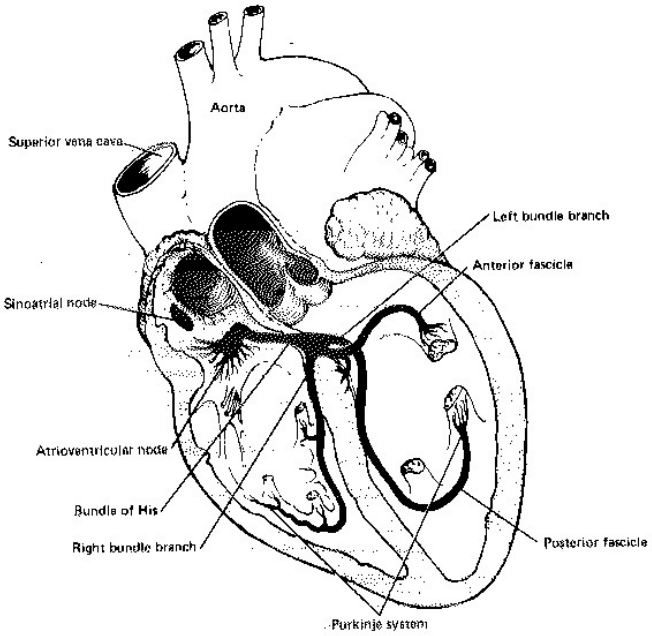

Figure 1.3 The impulse generating and conducting systems.

1.4 Surface Electrocardiograms (Surface-ECG)

The standard 12-lead ECG is a simple and noninvasive investigation that displays the electrical signal generated by the heart during the cardiac cycle. P wave of the ECG corresponds to atrial activation and QRS complex corresponds to ventricular activation. A typical lead surface-ECG is shown in Fig. 1.4 presenting the different waves appearing in each heart beat.

1.5 Arrhythmias: Atrial Fibrillation (AF)

An arrhythmia is a disorder of the regular rhythm of the heart beating. These irregular rhythms may indicate minor or serious problems due to abnormalities of the heart muscle, valves or arteries. Nevertheless, arrhythmias can also take place in a healthy heart, and be of minimal consequence.

Arrhythmias can be classified as ventricular or supraventricular depending on where they occur and also depending on how fast the irregular beats are, they are divided in bradycardia (too slow, less than 60 beats per minute) and tachycardia (too fast, more than 100 beats per minute).

Atrial fibrillation is a supraventricular arrhythmia that causes a fast and irregular rhythm. Instead of the regular initiation of the heart beat in the sinus node, there are more than one place where the electrical impulse starts in the atria. Electrical wavefronts spread out in the atria randomly or following patterns still unknown. Some studies have tried to clarify the multiple wavefronts hypothesis [1,5,6], however, it still remains as an interesting issue to evaluate spatial and temporal organization of atrial electrical activity during AF.

Although atria fail to maintain a regular pattern of depolarization, ventricles continue to depolarize in a normal pattern beginning in the AV node and spreading down to the ventricles through the normal paths, the cells

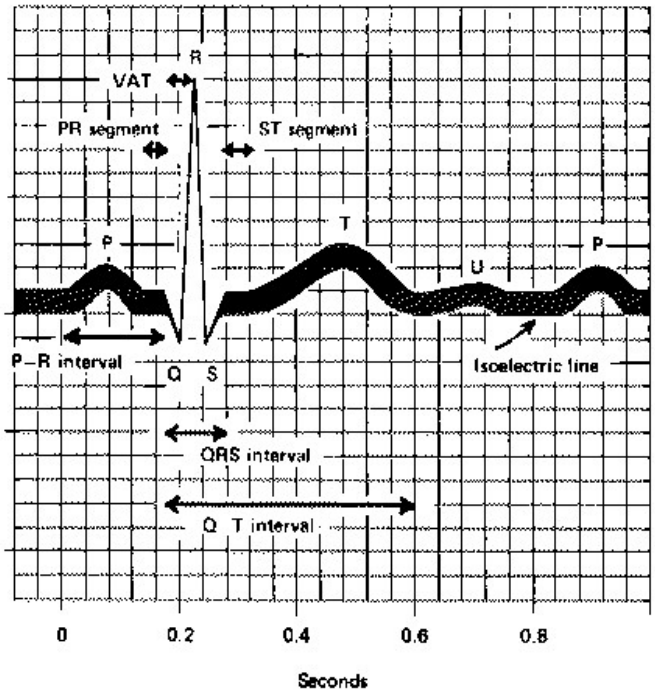

Figure 1.4 Typical lead surface-ECG.

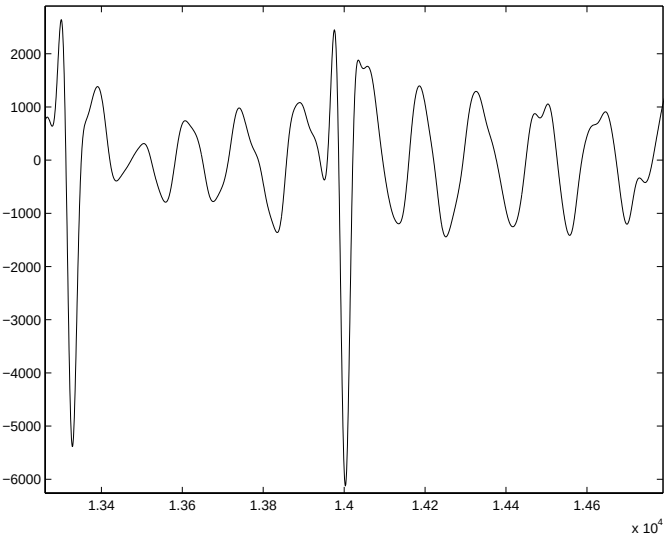

Figure 1.5 Lead V1 surface-ECG during AF.

of the bundle of His are activated and the impulse spreads by the Purkinje fibers to activate the ventricles. The rate of ventricular activation is often quite high and nearly always irregular due to the fact that many waves of fibrillation from the atria reach the AV node with an irregular and unknown pattern. Fig. 1.5 shows lead V1-surface ECG from a patient during atrial fibrillation. Instead of a P-wave representing the atria activation, five to seven waves per heart beat can be seen. The QRS-complex, ventricle activation, keeps the same shape though.

There are two different kinds of AF, Paroxysmal atrial fibrillation (PAF)

which starts and finishes spontaneously and Chronic Atrial Fibrillation (CAF) which persists until some clinical intervention causes its end, but never finishes spontaneously.

1.6 Cardiac Catheterization

A catheter is a long, thin and flexible tube that is introduced from the arm or the leg and passed through the blood vessels to the heart. Cardiac Catheterization may provide the most precise diagnosis in the majority of heart diseases.

In following chapters, we will describe the kind of catheters used in the present study to acquire endocardial electrograms from different points situated inside the heart. Always this catheter was motivated by clinical purpose.

2. Previous studies and motivation

Despite the fact that atrial fibrillation is one of the most common cardiac arrhythmias in man, the mechanisms maintaining this arrhythmia have not yet been satisfactorily clarified. In a paper published in 1962, Moe presented his so-called multiple wavelet hypothesis to explain the characteristics of atrial fibrillation [1]. According to this hypothesis, atrial fibrillation is maintained by the coexistence of a number of independent activation waves, called wavelets, that travel randomly through the atrial myocardium around multiple islets or strands of non-excitable tissue.

By endocardial activation mapping, Allessie and co-workers have confirmed Moe's hypothesis as a basis of acetylcholine-induced atrial fibrillation in isolated canine hearts [2]. The same group has shown, by high density epicardial activation mapping during cardiac surgery, that during electrically induced atrial fibrillation in patients with Wolff-Parkinson-White syndrome, the right atrium is activated by one or multiple activation waves propagating in different directions [3]. They identified three types of right atrial activation patterns, characterized by different numbers and dimensions of the intra-atrial re-entrant circuits.

Another study, performed by Cox and co-workers, included epicardial activation mapping of electrically induced atrial fibrillation both in dogs with created mitral regurgitation and in patients with Wolff-Parkinson-White syndrome [4]. The whole epicardial surface of both the right and the left atria was mapped using 208 electrodes in the animal set-up and 160 electrodes in the clinical set-up. The study demonstrated that multiple wave fronts, nonuniform conduction, bidirectional block and large re-entrant circuits occurred during induced atrial fibrillation. Small re-entrant circuits, however, were not reported by the investigators, possibly due to the limited spatial resolution.

The role of the multiple wavelet hypothesis in chronic atrial fibrillation in man, has been addressed in a study where the tendency for wave fronts to follow paths of previous excitation, so-called linking, was examined by analyzing atrial endocardial electrograms acquired using an orthogonal catheter [5]. In a majority of the patients, the investigators found groups of consecutive atrial beats where the direction of activation of each beat was within 30° of the previous beat and, furthermore, that this finding was consistent from the first minute of recording to the second. Their conclusion was that atrial activation during chronic atrial fibrillation in man is not entirely random.

To further investigate the degree of spatial and temporal organization of atrial activation, a method using a temporal averaging technique, that identifies characteristic activation patterns of the atria, has been reported in 1996 [6,9]. By applying the method in patients with CAF, three types of preferable activation patterns were identified: firstly, consistent activation with impulses originating from a specific site within the recording area, secondly, consistent activation with a preferable propagation direction, and finally, inconsistent or random activation. Moreover, an evaluation of temporal characteristics of the individual beats and atrial activations has been

developed applying a state-space realization technique in order to fit a multivariate impulse response model to data from multiple simultaneously acquired atrial electrograms [8]. Although the method [6,9] has proven to be a reliable tool for identifying atrial areas with consistent activation during fibrillation and electrograms have been locally and successfully predicted [8], it remains a relevant issue to evaluate spatial and temporal organization with data acquired from other parts of the heart in order to adequately characterize this arrhythmia.

Furthermore, defects in interatrial conduction in patients with AF have been addressed in two studies [13,14]. Afterwards, our group observed that during direct impulse conduction, using cardiac catheters and electrical stimulation technique, five patients out of 21 prone to attacks of atrial fibrillation often had evidence of delayed impulse conduction between the right and the left atrium [7]. However, patients with no previous AF didn't show any delay in conduction.

3. The objectives of the present study

- Endocardial electrograms from coronary sinus inside the heart can be seen as outputs of a system which input is the electrical impulse generated in the sinus node. Recently, atrial activity from epicardial electrograms has been modeled as an impulse response (the input can not be measured) with very good results in local predictions during sinus rhythm [8]. Also, a similar method has been applied to model P-waves from surface-ECG (recorded using modified Frank leads) and to classify them as normal or showing a conduction defect in the atria [11].

  In our study, chapter 5, we applied the same *impulse response methods* to reproduce atrial activity in endocardial electrograms from coronary sinus during sinus rhythm and during atrial fibrillation, comparing both cases.

- Considering endocardial electrograms as inputs (from inside the heart) and surface-ECG as outputs (from outside the heart), Subspace Model Identification (SMI) methods were applied in chapter 6. Success in predicting lead V1 surface-ECG from data obtained during catheter measurement would show an *input-output relation among signals from inside and outside the heart*.

- Apply correlation analysis and system identification tools to study *spatial and temporal propagation of atrial activation* along coronary sinus during paroxysmal atrial fibrillation and during sinus rhythm in different patients.

  Since the sensor (catheter) used is placed in the posterior left part of the heart, in the groove between left atrium and left ventricle, with one pole in the orifice of coronary sinus inside right atria, mechanisms of impulse conduction between right and left atria can be derived. Previous studies [13,14,7] have shown that patients prone to attacks of atrial fibrillation often had evidence of delayed impulse conduction between the right and the left atrium. However, only a visual analysis of individual heartbeats was done. In this master thesis, chapter 7, we have analyzed large intervals including many heartbeats and we have applied mathematical tools to study spatial and temporal propagation of atrial activation.

4. Materials and methods: Catheterization

Seven patients with paroxysmal atrial fibrillation (PAF) were included in the study, six of them measured during PAF and one measured during sinus rhythm (SR). The clinical characteristics of the patients are shown in Table 4.1. No anesthesia was used except Diazepam 2.5-5 mg intravenous injection when needed.

Table 4.1 Clinical Characteristics of the patients

Patient	*Sex* *M/F*	*Age* (*years*)	*Cardiac Rhythm*
1	M	52	PAF
2	M	22	PAF
3	M	56	PAF
4	M	48	PAF
5	M	50	PAF
6	M	46	PAF
7	F	58	SR

PAF= Paroxysmal Atrial Fibrillation.

Endocardial electrograms were simultaneously acquired with a commercially available standard 10 polar catheter placed in the coronary sinus (cs), the pole closest to right atrium being in the orifice of coronary sinus (Pole number 10). This catheter was always motivated by the clinical procedure. A DAIG 6F Decapolar CSL catheter (catalogue number 401400) was used in the first 6 patients, measured during PAF. Each pole was 1 mm wide and the distance between the electrodes 5 mm. Therefore, the average distance between electrodes was considered 6 mm. For Patient 7, measured during SR, a BARD 6F Decapolar Dynamic XT (catalogue number 201101) was used, with electrode average spacing 2, 5, 2 mm alternatively.

Also, 12-lead body surface recordings (surface-ECG) were made using commercially available standard ECG electrodes. Only lead V1 was used in this study as a reference to distinguish ventricle and atrial activation in endocardial electrograms. Each recording consisted of 10 unipolar electrograms from cs and lead V1 surface-ECG, simultaneously acquired with a sampling rate of 1 kHz, no filtered and A/D converted with a resolution of 12 bits.

The catheter was connected to the BARD Cardiac Mapping System, used to acquire and record the signals. The number of seconds recorded for each patient are presented in Table 4.2.

First three patient recordings were acquired with the following protocol: the first 30 seconds and the last 30 seconds were obtained with no artificial pacing but the remainder 30 seconds in between were measured while artificial atrial pacing performed at a pacing rate of 25 ms less than the

Table 4.2 Characteristics of recordings for each patient.

Patient	*Poles included*	*Pacing poles*	*Duration* $NP + P$ *(seconds)*
1	all	1-2	58+32
1	all	5-6	60+31
1	all	9-10	60+30
2	all	1-2	66+29
2	all	5-6	61+30
2	all	9-10	60+30
3	all	1-2	62+31
3	all	5-6	62+31
4	4,6,8,10	none	42+0
5	1,4,6,8,10	none	14+0
6	1,4,6,8,10	none	11+0
6	1,4,6,8,10	none	28+0
7	all	none	64+0
7	all	none	65+0

NP= Time (s) of recordings without artificial pacing.
P= Time (s) of recordings during artificial pacing between electrodes shown in column 'Pacing Poles'.

mean interval of atrial fibrillation (measured during one minute) using two poles (1-2, 5-6 or 9-10) of the coronary sinus catheter connected to an external heart stimulator. Recordings from Patients 4, 5 and 6 were acquired without any artificial pacing.

Considering that our analysis method is based on similarity of adjacent signals in the catheter, bipolar electrograms have been discarded although noise-free unipolar electrograms are hard to acquire in the operating room.

5. Reproduce atrial activations applying an impulse response method

5.1 Objective

We have applied impulse response identification methods to reproduce atrial activations in ten signals adquired simultaneously from the poles of a sensor (catheter) placed in the coronary sinus inside the heart. Results during sinus rhythm and during AF are presented in order to find out differences between both obtained models.

5.2 Signal analysis

The mean signal level was subtracted and a band-pass filter was also applied to all recordings from coronary sinus catheter poles.

Afterwards, we arranged data in intervals of N samples (ms), being N the number of samples in each atrial activation. Only atrial activations were included in the identification data. The first sample of each interval in each signal was forced to be zero.

5.3 System identification method

We have applied a state-space identification method based on the Markov parameters H_k, which are the coefficient matrices of the impulse response or the transfer function $H(z)$.

$$H(z) = \sum_{k=0}^{\inf} H_k z^{-k} \tag{5.1}$$

This algorithm was introduced by Ho and Kalman in 1966 [16] and reformulated by Kung in 1978 [20] via the singular value deecomposition. Later on, it was extended by Juang and Pappa in 1985 [17] and Bayard in 1994 [15].

Our system is considered to be discrete and time-invariant of order n with the following state-space equations:

$$x_{k+1} = A_n x_k + B_n u_k \tag{5.2}$$

$$y_k = C_n x_k + D u_k \tag{5.3}$$

where:

x_k represents the states

u_k the input (impulse)

y_k the outputs. In our case, the outputs are the 10 endocardial electrograms from the 10 poles of the coronary sinus catheter.

The goal is to identify the matrices A_n, B_n, C_n and D using a finite output sequence $\{y_k\}_{k=1}^{N}$ considered as a impulse response where N is the length of the impulse response recording. First of all, we arranged the Markov parameters of the system to construct the following Hankel matrices:

$$H_{r,s}^{(k)} = \begin{pmatrix} H_{k+1} & H_{k+2} & \dots & H_{k+s} \\ H_{k+2} & H_{k+3} & \dots & H_{k+s+1} \\ \vdots & \vdots & \ddots & \vdots \\ H_{k+r} & H_{k+r+1} & \dots & H_{k+r+s-1} \end{pmatrix}, \quad k = 0, 1 \tag{5.4}$$

where:

r and s where chosen such that $k + r + s \leq N$

The Markov parameters of the Hankel matrices H_k are the sample values of the 10 poles recordings:

$$H_0 = \begin{pmatrix} y_1(0) \\ y_2(0) \\ \vdots \\ y_{10}(0) \end{pmatrix}, \quad H_1 = \begin{pmatrix} y_1(1) \\ y_2(1) \\ \vdots \\ y_{10}(1) \end{pmatrix}, \quad \dots \tag{5.5}$$

Therefore, s was chosen equal to ten times r in order to have square Hankel matrices.

The order of the model had to be determined a priori, thus, examining the ranks of $H_{r,s}^{(0)}$ the minimal realization will be obtained for order n if:

$$n = \text{rank}(H_{n,j}^0) = \text{rank}(H_{n+1,j}^0) = \text{rank}(H_{n+2,j}^0) = \dots \tag{5.6}$$

where:

$j = n,\ n+1,\ n+2,\ \dots$

Computing the singular value decomposition (SVD) of $H_{r,s}^0$

$$H_{r,s}^0 = U \Sigma V^T \tag{5.7}$$

we can determine the order n of the system looking into its singular value sequence σ_k as shown in Fig. 5.1 to select an appropriate reduced model order.

The algorithm proposed by Juang and Pappa [17] to determine the state-space model of the n order system with m inputs and p outputs is :

$$A_n = \Sigma_n^{-1/2} U_n^T H_{r,s}^{(1)} V_n \Sigma_n^{-1/2} \tag{5.8}$$

$$B_n = \Sigma_n^{1/2} V_n^T E_u \tag{5.9}$$

$$C_n = E_y^T U_n \Sigma_n^{1/2} \tag{5.10}$$

$$D = H_0 \tag{5.11}$$

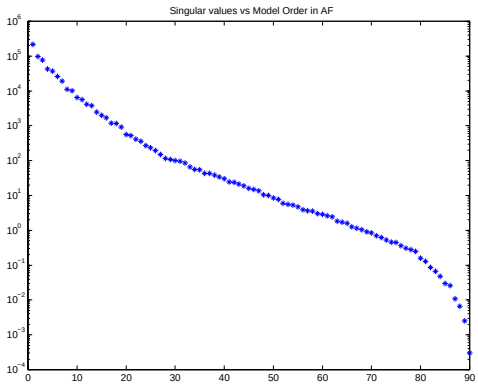

Figure 5.1 Singular values versus model order.

where:

$E_y^T = [I_{p\times p} \quad 0_{p\times(r-1)p}]$

$E_u^T = [I_{m\times m} \quad 0_{m\times(s-1)m}]$

$m = 1$ (number of inputs)

$p = 10$ (number of outputs)

$\Sigma_n = \text{diag}\{\sigma_1, \sigma_2, \ldots, \sigma_n\}$

$U_n =$ matrix of first n columns of U

$V_n =$ matrix of first n columns of V

5.4 Validation

In order to evaluate the model misfit, firstly we compare the model response and the measured response by plotting both together. Secondly, the residuals between each model output and the real output has been calculated as:

$$\varepsilon_k = \hat{H}_k - H_k = C_n A_n^{k-1} B_n - H_k \ , \quad k = 1,\ 2, \ldots,\ N. \tag{5.12}$$

Also the residuals are presented for each output to verify that all system dynamics were introduced in the model.

Finally, the relative prediction error has been calculated as:

$$\text{rpe} = \frac{\|\varepsilon^T \varepsilon\|_2}{\|H^T H\|_2} \tag{5.13}$$

where the residuals between the model output and the real output has been calculated as presented above and then grouped in a unique matrix as :

$$\varepsilon = (\varepsilon_1\ \varepsilon_2\ \ldots\ \varepsilon_N) \in \Re^{p\times N} \tag{5.14}$$

and the measured data has been also expressed in a unique matrix as:

$$H = (H_1\ H_2\ \ldots\ H_N) \in \Re^{p\times N} \tag{5.15}$$

5.5 Results

A typical experiment during sinus rhythm is presented in Figs. 5.2 to 5.11. Each figure shows with a dashed line the model output and with a solid line the measured data. Residual in each case are presented with a dotted line. The rpe was 0.0008 and the model order in this experiment was 23th.

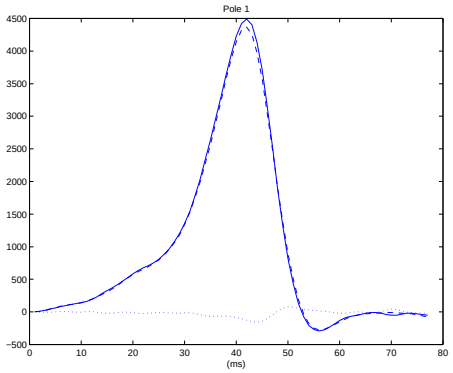

Figure 5.2 Pole 1 (SR).

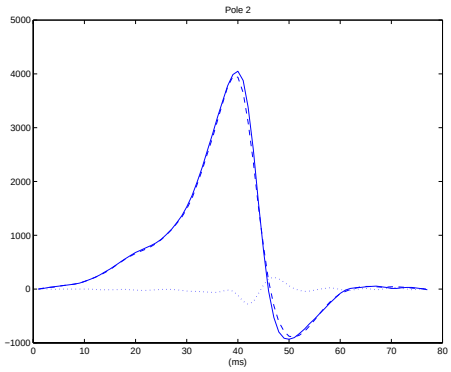

Figure 5.3 Pole 2 (SR).

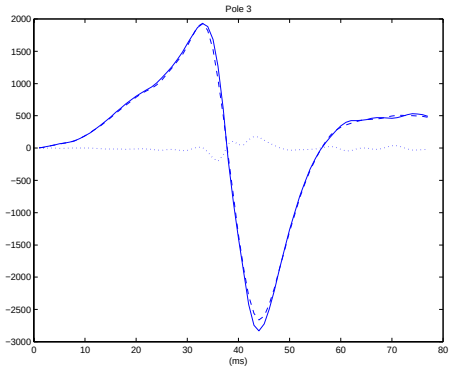

Figure 5.4 Pole 3 (SR).

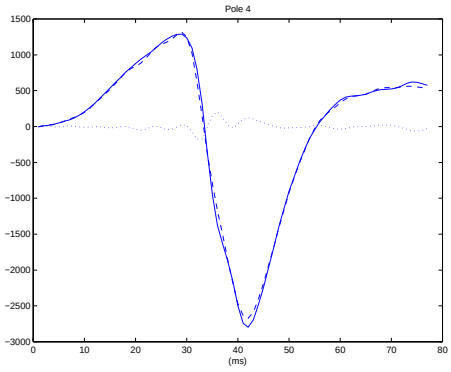

Figure 5.5 Pole 4 (SR).

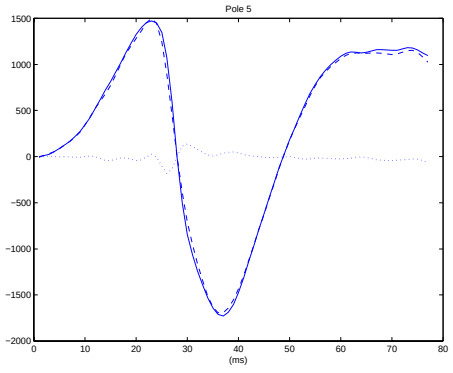

Figure 5.6 Pole 5 (SR).

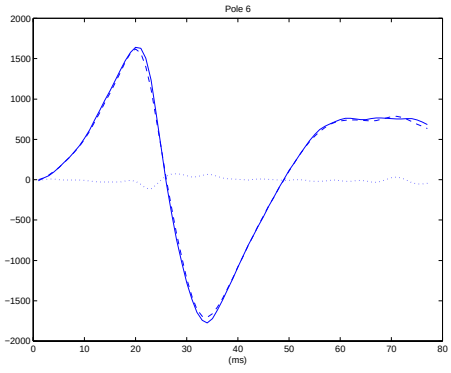

Figure 5.7 Pole 6 (SR).

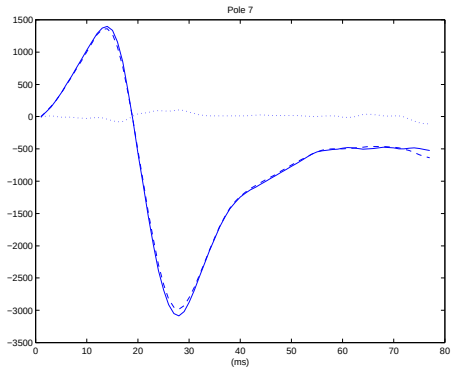

Figure 5.8 Pole 7 (SR).

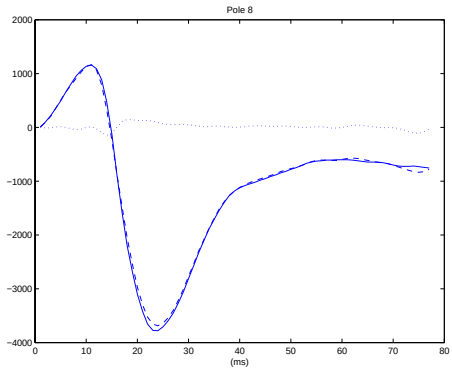

Figure 5.9 Pole 8 (SR).

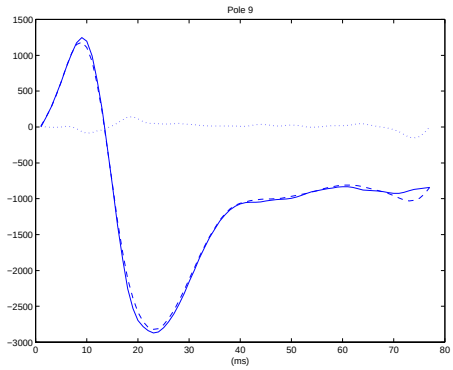

Figure 5.10 Pole 9 (SR).

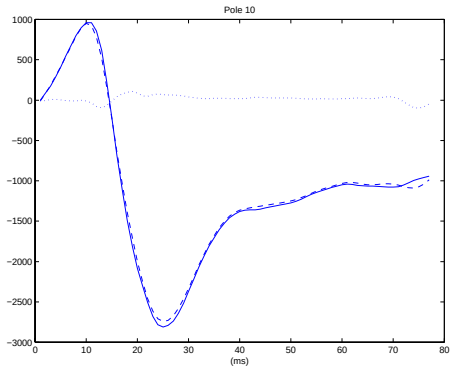

Figure 5.11 Pole 10 (SR).

Secondly, a typical experiment during atrial fibrillation is presented in Figs. 5.12 to 5.21. Each figure shows with a dashed line the model output and with a solid line the measured data. Residual in each case are presented with a dotted line. The rpe was 0.0009 and the model order in this experiment was 30th.

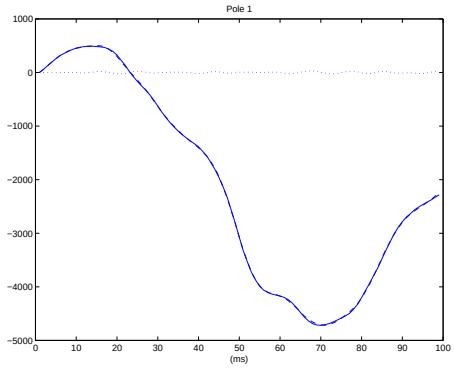

Figure 5.12 Pole 1 (AF).

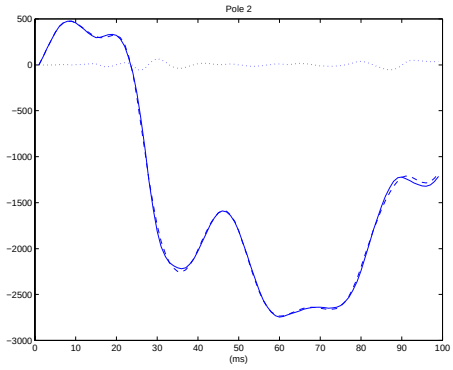

Figure 5.13 Pole 2 (AF).

Finally, the relative prediction error and the singular value sequence are presented for various model orders in figures 5.22 and 5.23 in the case of sinus rhythm and in figures 5.24 and 5.25 in the case of atrial fibrillation.

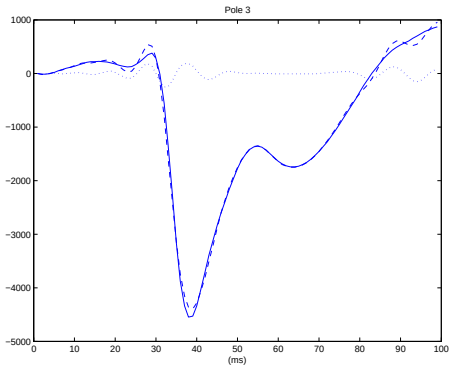

Figure 5.14 Pole 3 (AF).

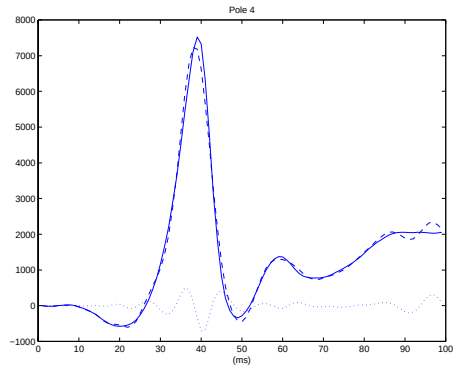

Figure 5.15 Pole 4 (AF).

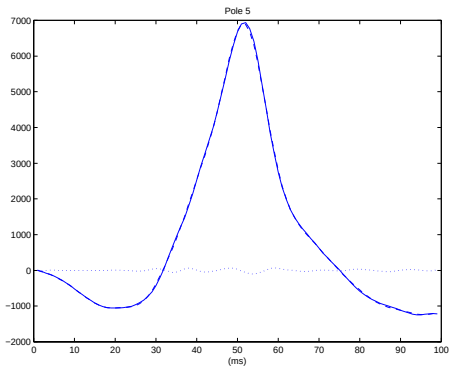

Figure 5.16 Pole 5 (AF).

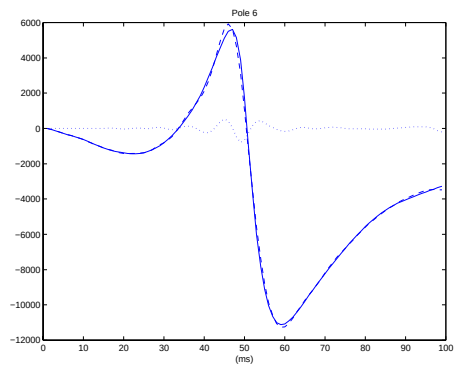

Figure 5.17 Pole 6 (AF).

5.6 Conclusions

The resulting models have presented high accuracy in reproducing atrial activity locally. However, these models can not be used to predict future atrial activations considering the different amplitude and shape of the ac-

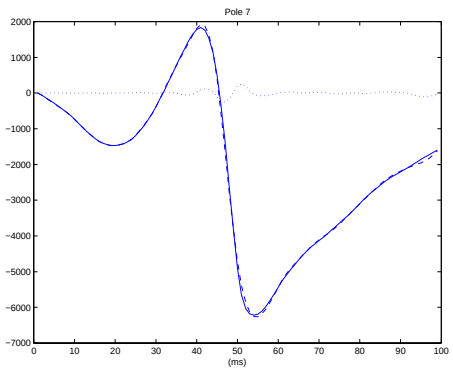

Figure 5.18 Pole 7 (AF).

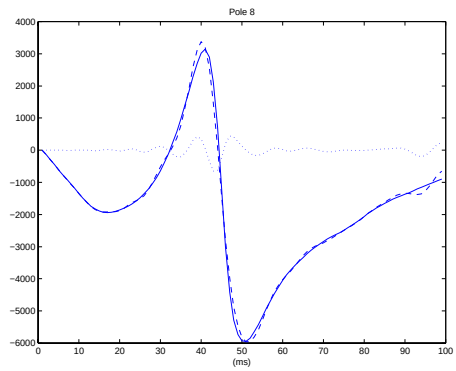

Figure 5.19 Pole 8 (AF).

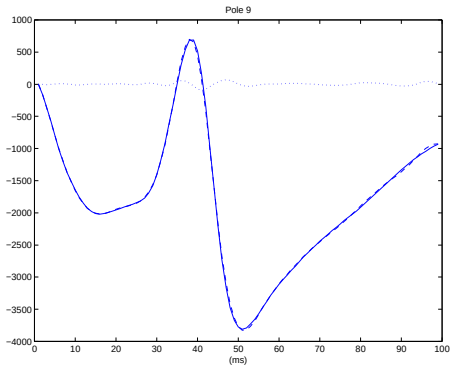

Figure 5.20 Pole 9 (AF).

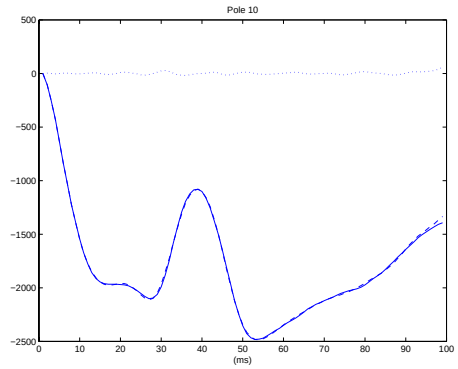

Figure 5.21 Pole 10 (AF).

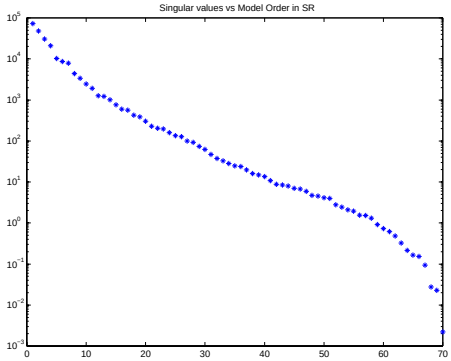

Figure 5.22 Singular value decomposition vs. model order (SR).

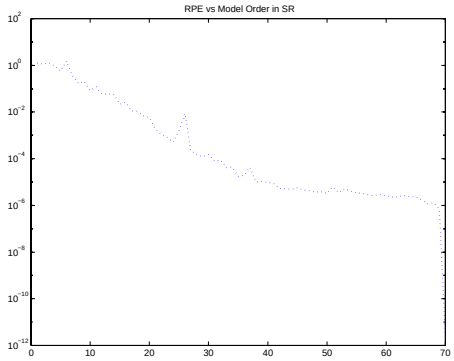

Figure 5.23 Relative prediction error vs. model order (SR).

tivations along a recording.

Nevertheless, future work could be done in obtaining models of atrial activations from endocardial electrograms of different patients in order to compare them. Differences related to the particular supraventricular arrhythmia suffered by each patient could be found out by computing these models. Mathematical analysis of atrial activations can identify differences

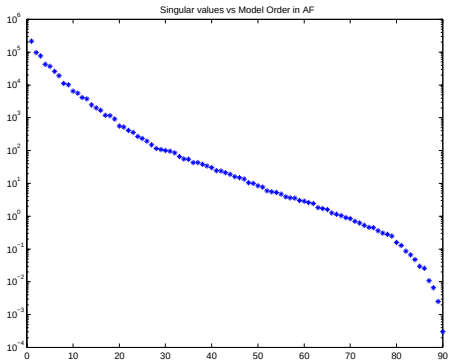

Figure 5.24 Singular value decomposition vs. model order (AF).

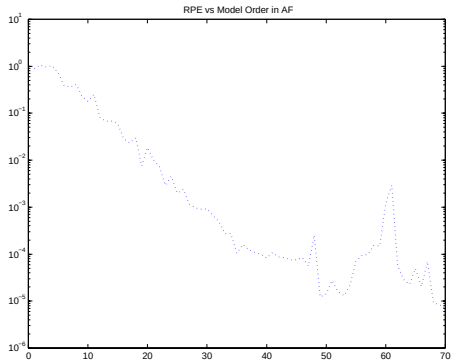

Figure 5.25 Relative prediction error vs. model order (AF)

that are not discovered by visual inspection.

Previous work has been done in classifying P-waves from surface-ECG obtaining 92.5% of the recordings correctly classified. Similar method could be applied to atrial activations in endocardial electrograms.

After applying the method in different activations some conclusions in practical aspects can be deduced. Firstly, it resulted a good choice to build square matrices. Thus, the number of rows should be equal to the number of block columns multiplied by the number of outputs: $s = r \times p$. We found out that other choices could estimate an unstable system. Secondly, it resulted better to force the first sample of each output to zero in order to pretend our data represent a real impulse response. Finally, the method was suitable for our problem since we did not need a measured input and no structure should be selected a priori, just the order of the system. In multivariable systems could result very long to select the structure of the system.

6. Subspace Model Identification (SMI) methods applied to endocardial and surface ECG

6.1 Objective

The goal of this chapter is to show an input-output relation among signals from inside (endocardial electrograms from poles in coronary sinus catheter) and outside (lead V1 surface-ECG) the heart. This was done applying a Subspace Model Identification (SMI) algorithm to build a state-space multi input single output model which is able to reproduce the output, lead V1 surface-ECG, with information from the inputs, the 10 unipolar electrograms from cs.

The algorithm applied is a member of the MIMO Output Error State Space (MOESP) class of algorithms developed the last decade by Verhaegen and Dewilde [18]. It is called PO-MOESP (Past Output instrumental variable method) and it solves the innovations model identification problem. The library of MOESP identification functions developed by Haverkamp [19] has been used to apply the PO-MOESP algorithm.

6.2 Signal Analysis

The mean signal level was subtracted and a band-pass filter was also applied to all recordings, both endocardial and surface ECG. Afterwards, data was split in two intervals for estimation and validation.

6.3 PO-MOESP Algorithm

This algorithm solves the innovations model identification problem. MOESP methods are closely related to Ho and Kalman [16] and Kung [20] algorithms for the realization method for state-space systems. However, a general input is used in PO-MOESP instead of the impulse used in those methods.

The innovation model identification problem is:

$$x_{k+1} = Ax_k + Bu_k + w_k \tag{6.1}$$

$$y_k = Cx_k + Du_k + v_k \tag{6.2}$$

where:

$x_k \in \Re^n$ represents the states

$u_k \in \Re^{10}$ represents the input data (endocardial electrograms from cs)

$y_k \in \Re$ represents the output data (lead V1 surface-ECG)

n is the order of the system

Two different noise sources are affecting the output: v_k is a measurement noise and w_k is a process noise. Both are white noise signals with zero-mean and statistically independent of u_k. Their covariance matrices are:

$$E\{\begin{pmatrix} w_k \\ v_k \end{pmatrix} \begin{pmatrix} w_k^T & v_k^T \end{pmatrix}\} = \begin{pmatrix} Q & S \\ S^T & R \end{pmatrix} \delta_{k,l} \tag{6.3}$$

where:

$$\delta_{k,l} = \begin{cases} 0 & k \neq l \\ 1 & k = l \end{cases} \tag{6.4}$$

An equivalent model form is called the innovations model form:

$$\hat{x}_{k+1} = A\hat{x}_k + Bu_k + Ke_k \tag{6.5}$$
$$\hat{y}_k = C\hat{x}_k + Du_k \tag{6.6}$$
$$y_k = \hat{y}_k + e_k \tag{6.7}$$

where:

e_k is a white noise signal independent of the past values of the input and output. It is called the innovation.

K is called the Kalman filter gain. For every choice of v_k and w_k there is only a matrix K and a white moise e_k that maintain the same relation input-output.

$\hat{y}_k$ is the minimum variance estimate of the outut y_k.

The algorithm steps to solve this problem are the following:

1. Build the Hankel matrices of the input and output data as shown bellow:

$$U_{i,j,N} = \begin{pmatrix} u_i & u_{i+1} & \cdots & u_{i+N-1} \\ u_{i+1} & u_{i+2} & \cdots & u_{i+N} \\ \vdots & \vdots & \ddots & \vdots \\ u_{i+j-1} & u_{i+j} & \cdots & u_{i+j+N-2} \end{pmatrix} \tag{6.8}$$

$$Y_{i,j,N} = \begin{pmatrix} y_i & y_{i+1} & \cdots & y_{i+N-1} \\ y_{i+1} & y_{i+2} & \cdots & y_{i+N} \\ \vdots & \vdots & \ddots & \vdots \\ y_{i+j-1} & y_{i+j} & \cdots & y_{i+j+N-2} \end{pmatrix} \tag{6.9}$$

Also, the Hankel matrices of the instrumental variables Z which are the combination of the past input and past output data:

$$Z = \begin{pmatrix} U_{0,i,N} \\ Y_{0,i,N} \end{pmatrix} \tag{6.10}$$

$$U_{0,i,N} = \begin{pmatrix} u_0 & u_1 & \dots & u_{N-1} \\ u_1 & u_2 & \dots & u_N \\ \vdots & \vdots & \ddots & \vdots \\ u_{i-1} & u_i & \dots & u_{N+i-2} \end{pmatrix} \tag{6.11}$$

$$Y_{0,i,N} = \begin{pmatrix} y_0 & y_1 & \dots & y_{N-1} \\ y_1 & y_2 & \dots & y_N \\ \vdots & \vdots & \ddots & \vdots \\ y_{i-1} & y_i & \dots & y_{N+i-2} \end{pmatrix} \tag{6.12}$$

2. Perform the following LQ factorization instead of the projection onto the orthogonal complement of $U_{i,j,N}$ and onto the instrumental variables: $Y_{i,j,N}\Pi^{\perp}_{i,j,N}\Pi_Z$

$$\begin{pmatrix} U_{i,j,N} \\ Z \\ Y_{i,j,N} \end{pmatrix} = \begin{pmatrix} U_{i,j,N} \\ U_{0,i,N} \\ Y_{0,i,N} \\ Y_{i,j,N} \end{pmatrix} = \begin{pmatrix} L_{11} & 0 & 0 & 0 \\ L_{21} & L_{22} & 0 & 0 \\ L_{31} & L_{32} & L_{33} & 0 \\ L_{41} & L_{42} & L_{43} & L_{44} \end{pmatrix} \begin{pmatrix} Q_1 \\ Q_2 \\ Q_3 \\ Q_4 \end{pmatrix} \tag{6.13}$$

3. In order to find the column space of the extended observability matrix Γ_{Ti}:

$$\Gamma_{Ti} = \begin{pmatrix} C_T \\ C_T A_T \\ C_T A_T^2 \\ \dots \\ C_T A_T^{i-1} \end{pmatrix} \tag{6.14}$$

compute the Singular Value Decomposition (SVD) of the matrix:

$$\begin{pmatrix} L_{42} & L_{43} \end{pmatrix} = U\Sigma V^T \tag{6.15}$$

The order n of the system can be estimated from the gap in the singular value sequence given by Σ.

4. Estimate $\hat{C}_T$ and $\hat{A}_T$ from U:

$$\hat{C}_T = \text{the upper l rows of } U_n \tag{6.16}$$

$$\hat{A}_T = U_1^{\dagger} U_2 \tag{6.17}$$

where:

U_n = the first n left singular vector of U

U_1 = the upper $(i-1)l$ rows of U_n

U_2 = the lower $(i-1)l$ rows of U_n

$U_1^{\dagger}$ = pseudo inverse of U_1

5. The estimation of B_T and D_T is done based on the fact that they depend linearly on the known A_T and C_T. This linear dependence is computed solving a linear least squares problem.

The index T in the state-space matrices refers to the determination of the system matrices up to the freedom in similarity transformation.

More details about the implementation of the PO-MOESP algorithm can be found in [19].

6.4 Validation

In order to evaluate the model misfit, firstly we study cross validation comparing the model response and the measured response by plotting both together. Different intervals for validation and for estimation were used.

Secondly, the residuals between each model output and the real output has been calculated as:

$$\varepsilon_k = \hat{y}_k - y_k, \quad k = 1,\ 2, \ldots,\ N. \tag{6.18}$$

They are presented to verify if all system dynamics were introduced in the model.

Finally, model validation was quantitatively computed in terms of percentage Variance Accounted For (VAF). It is a simple test quantity which gives a measure of the correctness of a model by comparing the estimated output of the model and output data.

$$\text{VAF} = (1 - \frac{(Y_N - \hat{Y}_N)^T (Y_N - \hat{Y}_N)}{Y_N^T Y_N}) \times 100\% \tag{6.19}$$

6.5 Results

A typical experiment for patient 1 during atrial fibrillation is presented in this section. Cross validation during three heart beats is presented in Fig. 6.1. The order of the model was selected a priori from the gap in the singular value sequence shown in Fig. 6.2. Therefore, 8^{th} order was selected resulting in a model with a percentage Variance Accounted For equal to 78.1%.

The misfit of the model is presented in Fig. 6.3. The QRS-complex is correctly estimated in all heart beats as it can be seen in the cross validation but the atrial fibrillation frequency was not capture in all heart beats. It can be due to different frequencies in atrial activity in signals from coronary sinus (inputs) and in surface-ECG signals (output).

Another example for patient 3 during atrial fibrillation is presented in Figs. 6.4 and 6.5. The first figure shows a fine estimation of the atrial activations since the second one presents some heart beats where the fibrillation frequency has not been properly estimated. The estimation error is presented in Fig. 6.6 and the singular value sequence in Fig. 6.7. The selection of the order of the system was based on the clear gap in this sequence, thus, 5th order was chosen. Percentage Variance Accounted For was in this case equal to 81.4%.

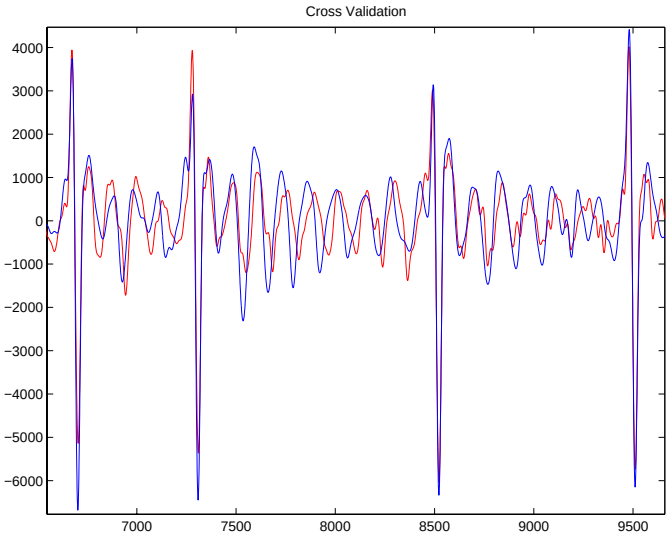

Figure 6.1 Cross validation, patient 1: Measured V1 (blue) and estimated V1(red) during three heart beats

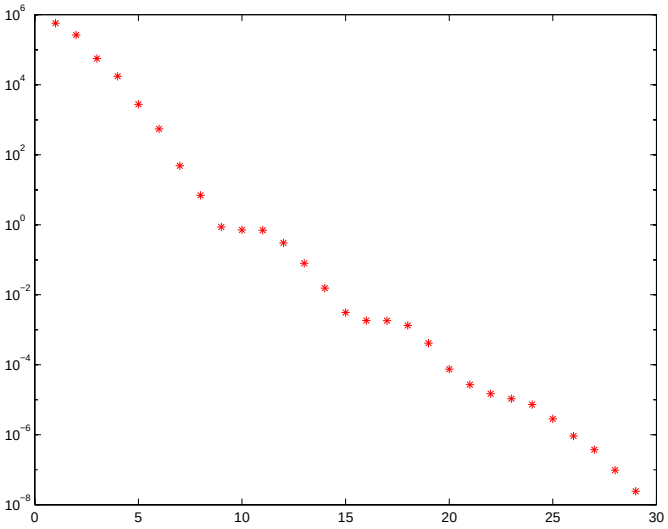

Figure 6.2 Singular value decomposition vs. model order, patient 1

6.6 Conclusions

An input-output linear relation among signals inside and outside the heart has been shown with no complete success in reproducing all the atria activations along different heart beats. Probably, better results could be obtained if we use as the input signals, endocardial electrograms from other parts in the atria. The coronary sinus catheter is placed in the back part of the atria and V1 is obtained from surface electrodes in the front part, thus, frequencies in atrial activations could be different.

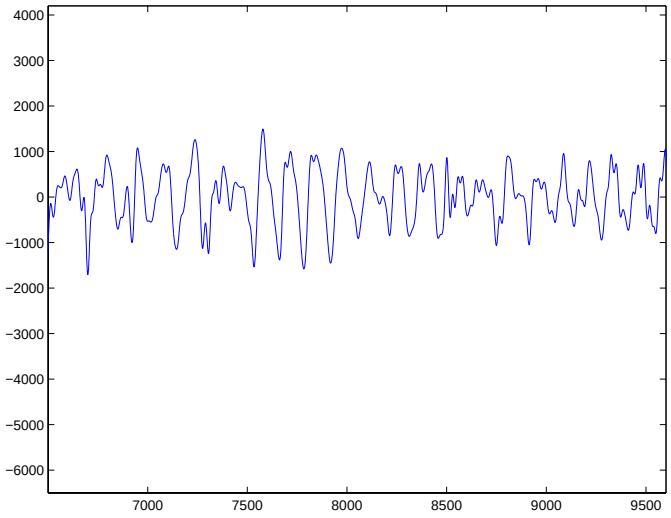

Figure 6.3 Error in the estimation of V1, patient 1

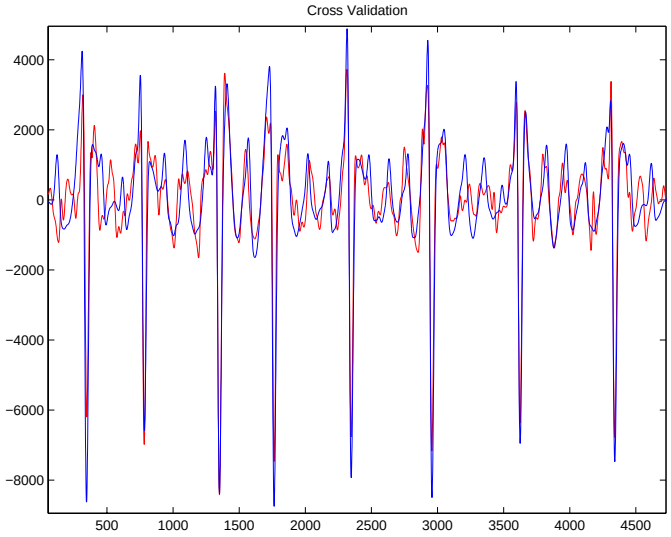

Figure 6.4 Cross validation, patient 3: Measured V1 (blue) and estimated V1(red) during three heart beats

Subspace Model Identification methods resulted excellent tools for multivariable systems because there is no need of selecting the structure of the system a priori. However, the order of the system has to be selected a priori but the singular value decomposition is a helpful tool that gives us the singular value sequence where we can find a large gap (not always very clear) to select the adequate reduced order model.

Nevertheless, to compute the Hankel matrices we needed to decide their number of block rows as a parameter in the algorithm, which is only required to be bigger than the order of the system. A wrong selection resulted in an unstable system. After some experiments applying this method, we could conclude that this selection was not obvious. In most of the cases, double the order of the system was needed to obtain a stable system.

Another conclusion after applying the method in different intervals and patient recordings was that we needed to use very large data intervals for

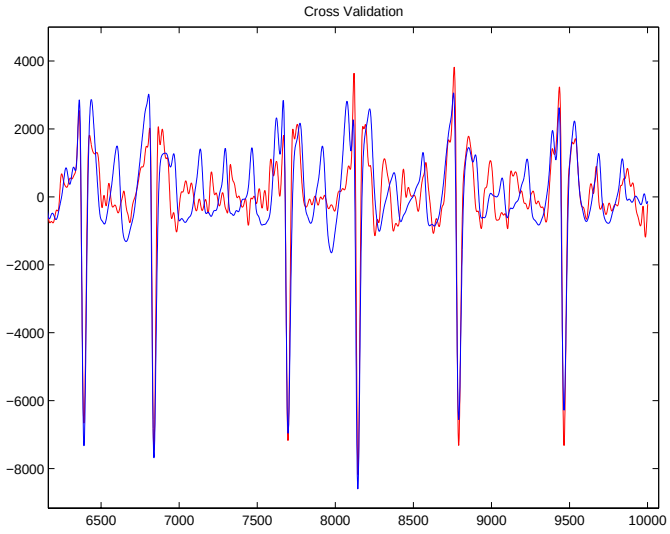

Figure 6.5 Cross validation, patient 3: Measured V1 (blue) and estimated V1(red) during three heart beats

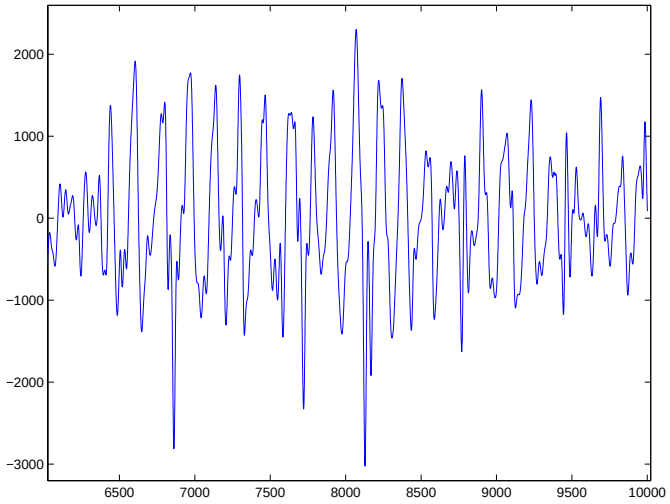

Figure 6.6 Error in the estimation of V1, patient 3

estimation to obtain a model with high accuracy. About twenty seconds recordings (include more than twenty heart beats) was a good selection.

Moreover, a narrow band pass filter was applied to the data in order to obtain these accurate models. The band frequency had to include the fibrillation frequency (from 5 to 13 Hz), thus, the band pass filter selected was from 5 to 30 Hz in most cases.

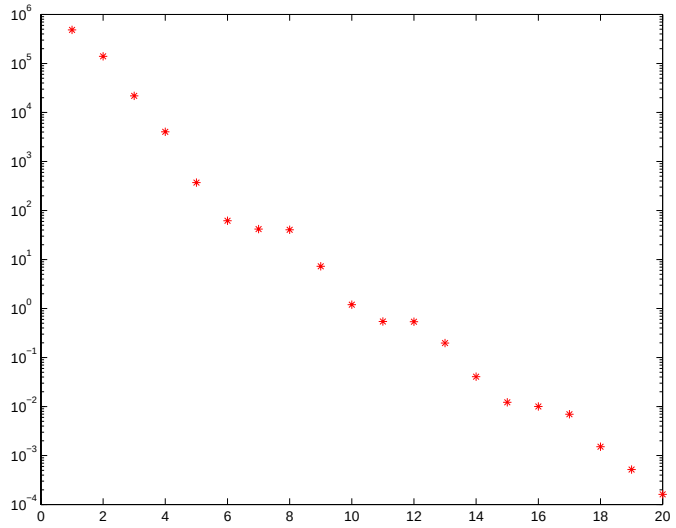

Figure 6.7 Singular value decomposition vs. model order, patient 3

7. Spatial and temporal propagation of atrial activity during AF and SR

7.1 Objective

Clarifying the mechanisms maintaining atrial activity during atrial fibrillation (AF), still remains as a relevant topic. The purpose of this chapter is to apply correlation analysis and system identification methods to study spatial and temporal propagation of atrial activation along coronary sinus (situated in the posterior left part of the heart, in the groove between left atrium and left ventricle) during paroxysmal atrial fibrillation (PAF) using data recorded catheter from 7 different patients. Furthermore, interatrial mechanisms of impulse conduction can be derived due to the position of coronary sinus.

7.2 Signal Analysis

After a visual analysis of each data set, some intervals of data have been manually discarded due to saturated signals when pole-tissue contact is not complete. Moreover, data very close to the end of the artificial pacing has also been rejected during the interval that signals from pacing poles did not reach their mean value. Besides, removal of a 50 Hz disturbance component emanating from power supplies was applied before handling the following four steps analysis.

7.3 Correlation analysis on complete signals

We computed the correlation function among signals along the coronary sinus catheter. The correlation function between two signals can be defined as the correlation coefficient $\rho(\tau)$ calculated for $\tau = -n, \ldots, -1, 0, 1, \ldots, n$. The correlation coefficient $\rho(\tau)$ was calculated shifting in time the first signal referring to the second signal τ samples (time shift $= \tau$ ms considering sampling rate equal to 1 kHz) as shown in the following equations.

$$\rho(\tau) = \frac{C_{xy}(\tau)}{\sqrt{|C_{xx}(\tau)|}\sqrt{|C_{yy}(\tau)|}} \tag{7.1}$$

where the sample covariances are defined according to:

$$C_{xx}(\tau) = \frac{1}{N-\tau}\sum_{i=1}^{N-\tau}(x_{i+\tau} - \bar{x}_{1+\tau,N})(x_i - \bar{x}_{1,N-\tau})^T \tag{7.2}$$

$$C_{xy}(\tau) = \frac{1}{N-\tau} \sum_{i=1}^{N-\tau} (x_{i+\tau} - \bar{x}_{1+\tau,N})(y_i - \bar{y}_{1,N-\tau})^T \tag{7.3}$$

and the sample means:

$$\bar{x}_{1,N-\tau} = \frac{1}{N-\tau} \sum_{i=1}^{N-\tau} x_i, \quad \bar{x}_{1+\tau,N} = \frac{1}{N-\tau} \sum_{i=1+\tau}^{N} x_i \tag{7.4}$$

$$\bar{y}_{1,N-\tau} = \frac{1}{N-\tau} \sum_{i=1}^{N-\tau} y_i, \quad \bar{y}_{1+\tau,N} = \frac{1}{N-\tau} \sum_{i=1+\tau}^{N} y_i \tag{7.5}$$

where:

N= total number of samples

τ= time shift in ms

Also the maximum of the correlation function is computed.

$$\tau_{\max} = \arg\max_{\tau}(\rho(\tau)), \quad \rho_{max} = \rho(\tau_{max}) \tag{7.6}$$

τ_{max} gives the time shift (in miliseconds) where both signals are most correlated, i.e., major similarity between these two signals is founded when one of them is shifted τ ms.

ρ_{max} gives the maximum correlation coefficient in a range from zero to one which means that correlation between signals is low or high respectively.

7.4 Calculating the excitation direction and velocity component

The correlation function has been calculated between one signal as reference and the signals measured by the remainding poles available in each data set. All signals were analyzed in order to choose the reference signal as the one that presented first activation by means of resulting positive time shifts in the maximum of the correlation function with the majority of the signals.

Information about the spatial propagation of electrical activity along coronary sinus can be extracted. The *excitation direction* can be inferred from the sign of τ_{max}. A positive time shift indicated propagation from the reference pole to the other pole used to calculate the correlation function, whereas a negative time shift denotes propagation towards the reference signal.

The *excitation speed* can be estimated from the absolute value of τ_{max}.

$$v_{r,x} = \frac{6|x-r|}{(\tau_{max})_{r,x}} \frac{m}{s} \tag{7.7}$$

where:

r = index of reference pole

x = index of second pole in correlation function

$(\tau_{max})_{r,x}$ = maximum in the correlation function between signals from poles r and x.

However, real speed can not be calculated due to signals are spatially limited to one dimension but no information is acquired from the other two dimensions in space. Therefore, electrical activity propagating in an oblique direction towards coronary sinus produces an erroneous speed calculation.

7.5 Substitution of ventricle response by a linear interpolation in all coronary sinus catheter signals

Considering that ventricular excitation affected our signals with higher amplitude than atrial excitation, previous results could be distorted by ventricular activity. Since we are only interested in atrial electrical activity, substitution of ventricle response was performed calculating its start and end as the limits of the QRS complex in lead V1 surface-ECG. Accurate estimation of QRS start and end was not necessary as long as the high magnitude of ventricle impulse is removed from the coronary sinus signals. Afterwards, a linear interpolation was calculated in between both estimated limits. An example of this substitution is presented in Figs.7.1 and 7.2 during one heart beat. Large difference in magnitude of ventricle and atrial response can be recognized.

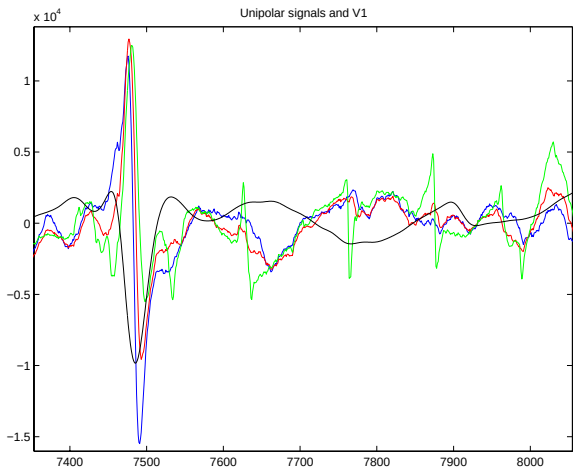

Figure 7.1 Real signals during one heart beat in Patient 3. Lead V1 surface-ECG (black) and coronary sinus signals from Poles 1-3 (colored).

7.6 Correlation analysis on signals with substituted ventricle response

First two steps, sections 7.3 and 7.4, were applied again but on the new signals. Notable differences on excitation velocity and direction were founded

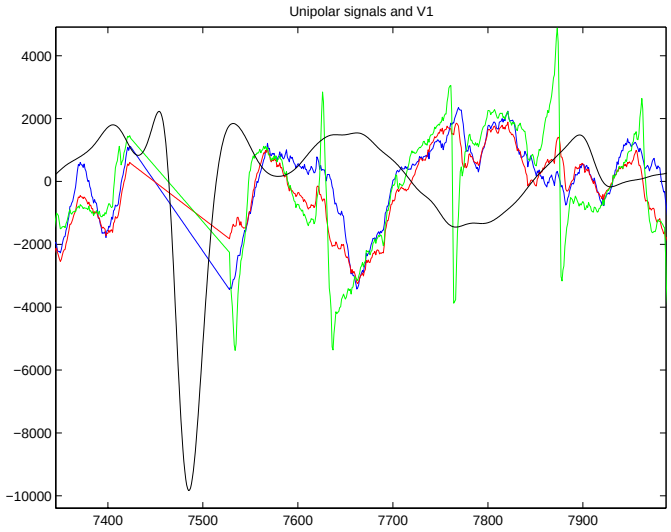

Figure 7.2 Signals with ventricle response removed during one heart beat in Patient 3. Lead V1 surface-ECG (black) and coronary sinus signals from Poles 1-3 (colored).

in most data sets. Therefore, it was proved that previous results were distorted.

We present an example of differences for patient 3 (data interval 4) in Figs. 7.3 and 7.4. The first figure gives the correlation function among original signals and the second one among signals with ventricle response substitued by a linear interpolation showing obvious differences in propagation direction and speed.

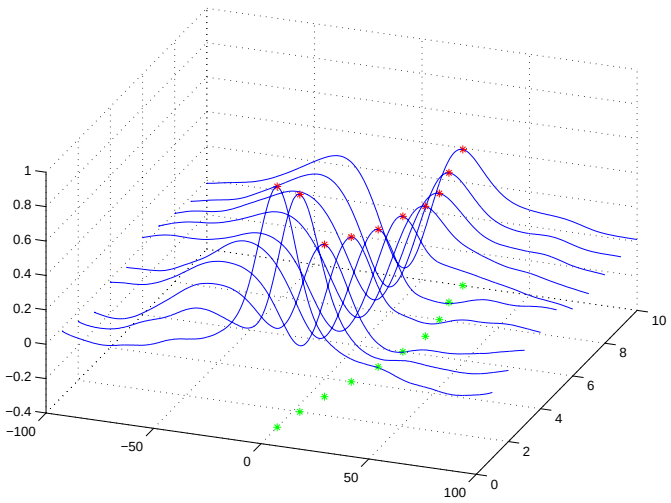

Figure 7.3 Correlation function for **original signals**(Patient 3, interval 4) between first Pole as reference and all the others. The maximum of each correlation function is shown as a * over the function and also its projection. X axis represents space: 1st to 10th Poles in the catheter. Y axis represents time shift and Z axis gives the value of the correlation coefficient.

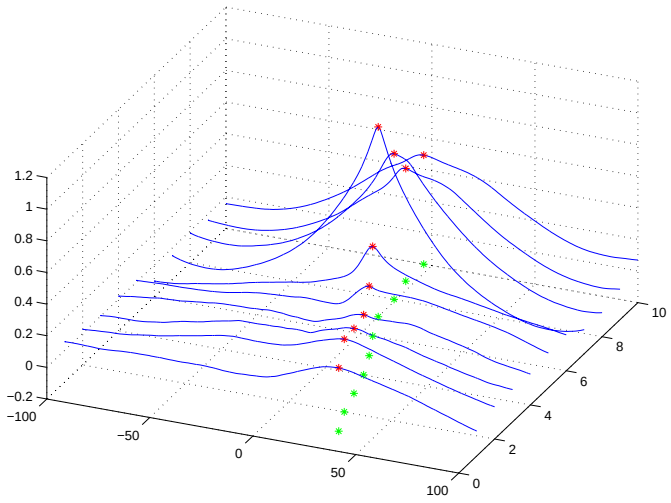

Figure 7.4 Correlation function for **signals with ventricle response substituted**(Patient 3, interval 4) between 8th Pole as reference and all the others. The maximum of each correlation function is shown as a * over the function and also its projection. X axis represents space: 1st to 10th Poles in the catheter. Y axis represents time shift and Z axis gives the value of the correlation coefficient.

7.7 System identification applied to verify previous results

Considering as inputs the closest poles to the output electrode, a simple linear model was fitted to data using least-squares method. The input-output delay was given by the results obtained from the correlation analysis. Our linear regression analysis is based on the model

$$y_{k,s} = \sum_{i=1}^{N} a_i y_{k-i,s} + \sum_{i=d_1}^{N} b_i y_{k-i,s-1} + \sum_{i=d_2}^{N} c_i y_{k-i,s+1} + e_k \tag{7.8}$$

where:

$s =$ space (number output pole)

$k =$ time (sample instant)

$d_1 =$ delay between y_s and y_{s-1} given by previous results in correlation analysis

$d_2 =$ delay between y_s and y_{s+1} given by previous results in correlation analysis

$e_k =$ additive errors, they are assumed to have the form:

$$E\{e_i\} = 0, \quad E\{e_i e_j\} = \sigma_e^2 \delta_{ij}, \quad \forall i, j \tag{7.9}$$

In ARX form:

$$A(q)y_s(t) = B(q)y_{s-1}(t-d_1) + C(q)y_{s+1}(t-d_2) \tag{7.10}$$

7.8 Model Validation

Model validation was quantitatively computed in terms of percentage Variance Accounted For and qualitatively by cross validation between real and estimated output.

Variance Accounted For (VAF) is a simple test quantity which gives a measure of the correctness of a model by comparing the estimated output of the model and output data.

$$\text{VAF} = (1 - \frac{(Y_N - \hat{Y}_N)^T (Y_N - \hat{Y}_N)}{Y_N^T Y_N}) \times 100\% \tag{7.11}$$

For least-squares case, it can be formulated in the following way:

$$\text{VAF} = \frac{\hat{Y}_N^T \hat{Y}_N}{Y_N^T Y_N} \times 100\% \tag{7.12}$$

Cross-validation was made applying input data not previously used in identification. After visual comparison between data and model output, i.e. Y and $\hat{Y}$, success or failure told us whether our system was time-invariant or not.

7.9 Results

Correlation function: excitation direction and speed

Results in correlation analysis showed consistent patterns in spatial and temporal propagation during atrial fibrillation in five patients out of six. All results were obtained using signals with ventricle response substituted.

Two wave fronts meeting somewhere inside the coronary sinus were identified in Patients 1 and 2. For example, Fig. 7.5 presents the correlation function for Patient 2 where the maximum spreads out in space (1st to 8th Pole in the catheter) increasing time shift from 0 to 45 ms and then decreasing again (from 8th to 10th Pole). Consequently, two different excitation directions were obtained confronting in Pole 8.

A unique consistent wave was found in Patients 3, 4 and 5. Fig. 7.6 shows results for Patient 3 where only one propagation direction appeared from 7th to 1st Pole increasing time shift from 0 to 33 ms.

No consistent spatial propagation was obtained for the last AF Patient.

Direction and speed of propagation resulted dependent on the patient. A summary of results for all patients is presented in Table: 7.1.

During sinus rhythm, the case presented higher values in the maximum of the correlation function than during AF and a unique wave as it is shown also in Table 7.1. The resulting correlation function is presented in Fig. 7.7.

Identification results

The models obtained exhibited high accuracy and low order (4th to 6th range). Results of typical experimental data and cross-validation simulation are presented in Fig. 7.8 (Patient 1, AF, 2 wave fronts, VAF= 96,1%),

Table 7.1 Maximum correlation coefficient range, excitation direction and speed in each data interval.

Patient/ Data interval	*Interval Duration* (ms)	ρ_{max} *range*	*Excitation direction*	*Excitation speed* (m/s)
1/1	30840	0.91 to 0.5	$1 \Leftarrow 2-3 \Rightarrow 8-9 \Leftarrow 10$	X/1.15/X
1/2	12014	0.93 to 0.45	$1 \Leftarrow 2-3 \Rightarrow 8-9 \Leftarrow 10$	X/1.11/X
1/3	15801	0.95 to 0.55	$1 \Leftarrow 2-3 \Rightarrow 7 \Leftarrow 8-9-10$	X/1.5/X
1/4	24401	0.96 to 0.49	$1-2-3 \Rightarrow 7 \Leftarrow 10$	1.1/0.82
1/5	6501	0.95 to 0.23	$1 \Leftarrow 2-3 \Rightarrow 7 \Leftarrow 10$	X/1.2/0.9
2/1	33701	0.68 to 0.08	$1 \Rightarrow 8 \Leftarrow 10$	0.93/0.63
2/2	8601	0.63 to 0.07	$1 \Rightarrow 8 \Leftarrow 9-10$	0.78/X
2/3	29800	0.52 to 0.15	$1 \Rightarrow 7 \Leftarrow 9-10$	1.16/1.33
2/4	8564	0.51 to 0.06	$1 \Rightarrow 6-7 \Leftarrow 10$	0.94/1
2/5	28752	0.59 to 0.11	$1 \Rightarrow 7-8$ *	0.78
3/1	23201	0.53 to 0.3	$1 \Leftarrow 5$	0.92
3/2	18251	0.54 to 0.16	$1 \Leftarrow 5$	0.6
3/3	29500	0.7 to 0.2	$1-2 \Leftarrow 7-8$	1.09
3/4	24960	0.76 to 0.16	$1 \Leftarrow 7-8$	0.77
4/1	19801	0.16 to 0.08	$4 \Leftarrow 10$	0.9
4/2	19701	0.22 to 0.07	$6 \Leftarrow 10$	0.92
5/1	5000	0.32	$4 \Rightarrow 6$	0.8
5/2	9464	0.23	$4 \Rightarrow 6$	0.92
6/1	11775	0.86 to 0.11	no patterns	X
6/2	28287	0.9 to 0.26	no patterns	X
7/1	19851	0.91 to 0.6	$1 \Leftarrow 8-9-10$	0.71
7/2	20001	0.94 to 0.65	$1 \Leftarrow 8-9-10$	0.71
7/3	23993	0.94 to 0.66	$1 \Leftarrow 8-9-10$	0.71
7/4	20001	0.95 to 0.66	$1 \Leftarrow 8-9-10$	0.71
7/5	28001	0.93 to 0.65	$1 \Leftarrow 8-9-10$	0.71
7/6	6866	0.95 to 0.68	$1 \Leftarrow 8-9-10$	0.74

1 to 10: stands by pole numbers in the coronary sinus catheter.
$\Leftarrow, \Rightarrow$: give the consistent direction patterns in propagation.
x-y :no time shift between x and y electrodes or smaller than 3 ms.
speed1/speed2 :each speed corresponds to each previous direction (arrow).
X: impossible speed calculation.
*: Poles 9 and 10 saturated.

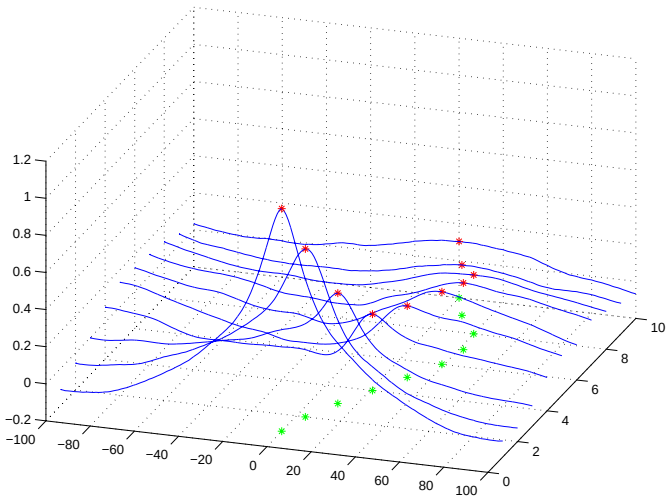

Figure 7.5 Correlation function (Patient 2, interval 1) between first Pole as reference and all the others. The maximum of each correlation function is shown as a * over the function and also its projection. X axis represents space: 1st to 10th Poles in the catheter. Y axis represents time shift and Z axis gives the value of the correlation coefficient.

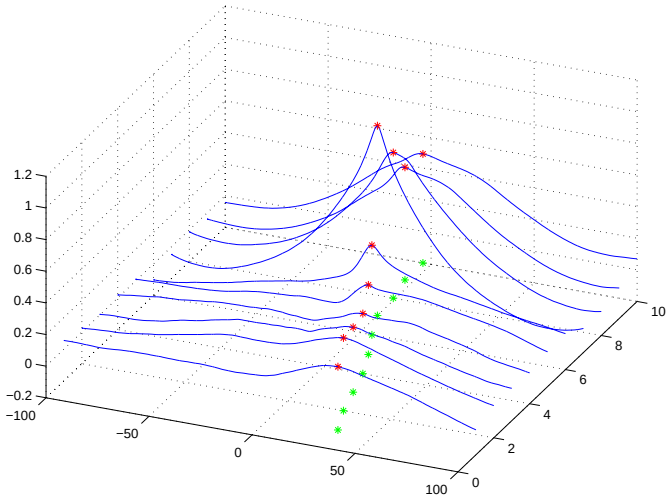

Figure 7.6 Correlation function (Patient 3, interval 3) between 7th Pole as reference and all the others. The maximum of each correlation function is shown as a * over the function and also its projection. X axis represents space: 1st to 10th Poles in the catheter. Y axis represents time shift and Z axis gives the value of the correlation coefficient.

Fig. 7.9 (Patient 3, AF, 1 wave front, VAF= 83,4%) and Fig. 7.10 (Patient 7, SR, VAF= 97,9%).

Bode diagrams pole 6-pole 7 and pole 8-pole 7 for the first patient are shown in Figs. 7.11. Also the coherence function in this case is presented in Fig. 7.12

Bode diagrams for the nine systems along the catheter are presented in Fig. 7.13 during sinus rhythm, patient 7, and the corresponding coherence functions for every pair input-output in Fig. 7.14.

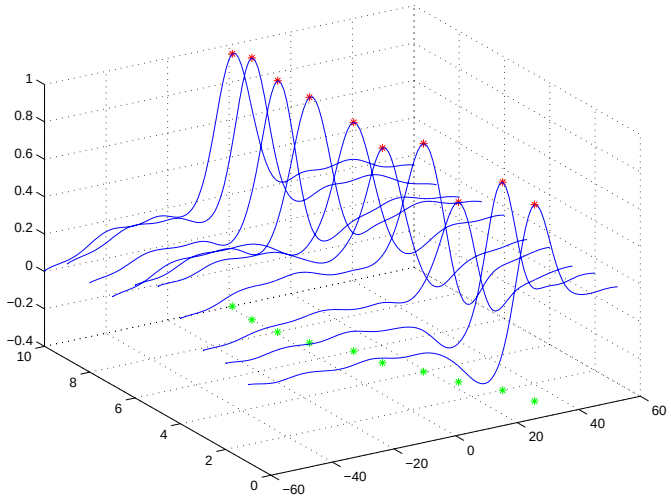

Figure 7.7 Correlation function (Patient 7, interval 2) between 9th Pole as reference and all the others. The maximum of each correlation function is shown as a * over the function and also its projection. X axis represents space: 1st to 10th Poles in the catheter. Y axis represents time shift and Z axis gives the value of the correlation coefficient.

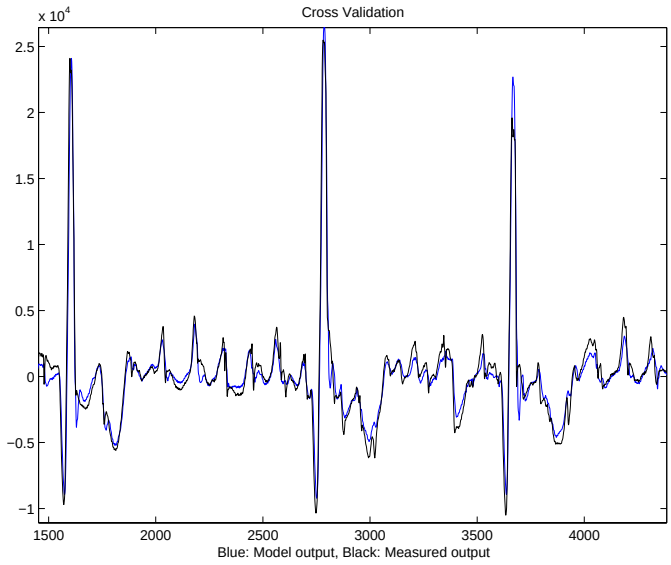

Figure 7.8 Accuracy of cross validation, Patient 1, AF. Output: 7th Pole, Inputs: 6th and 8th Poles, order=4, VAF= 93,1%.

7.10 Discussion

This study demonstrated consistency in electrical activity propagation during atrial fibrillation along coronary sinus in all cases with one exception. The value of the maximum correlation coefficient can be viewed as an average of all atrial activations in the interval studied. Thus, it could give us an idea of the percentage of activations that follow the patterns founded. However, tissue attenuation among poles and noise conditions could also reduce this maximum.

The findings regarding to two wave fronts in first two patients are compatible with excitation that follows the same patterns as expected during

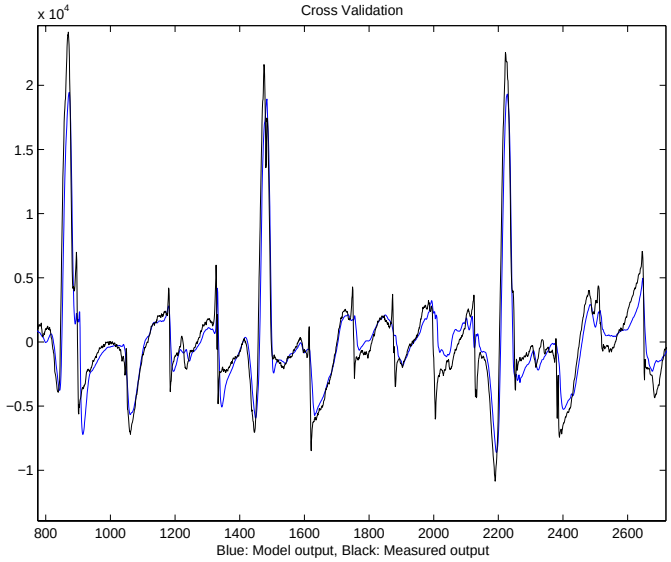

Figure 7.9 Accuracy of cross validation, Patient 3, AF. Output: 7th Pole, Inputs: 6th and 8th Poles, order=5, VAF= 83,4%.

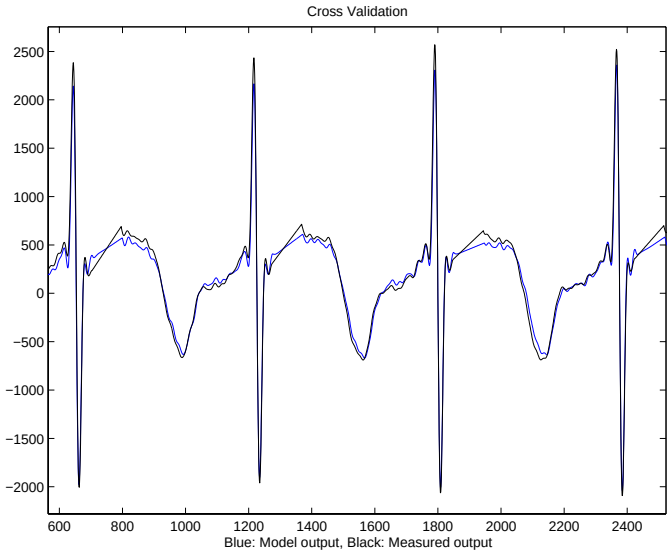

Figure 7.10 Accuracy of cross validation, Patient 7, SR. Output: 7th Pole, Inputs: 6th and 8th Poles, order=4, VAF= 97,9%.

SR, i.e., one wave front propagating from the roof of the left atrium and the other one coming from the right atrium by inferoposterior interatrial connections running in bundles or in the wall of coronary sinus. This is evidence of left atrial activation from right atrium during PAF. In any case, all results can be used to derive mechanisms of impulse conduction between right and left atrium due to the position of coronary sinus.

However, speed calculations were not conclusive due to signals are spatially limited to one dimension but no information is acquired from the other two dimensions in space. Therefore, electrical activity propagating in an oblique direction towards coronary sinus will produce an erroneous speed calculation. Interesting future work could be done applying the same procedure on signals spread out inside the atria in two and three dimen-

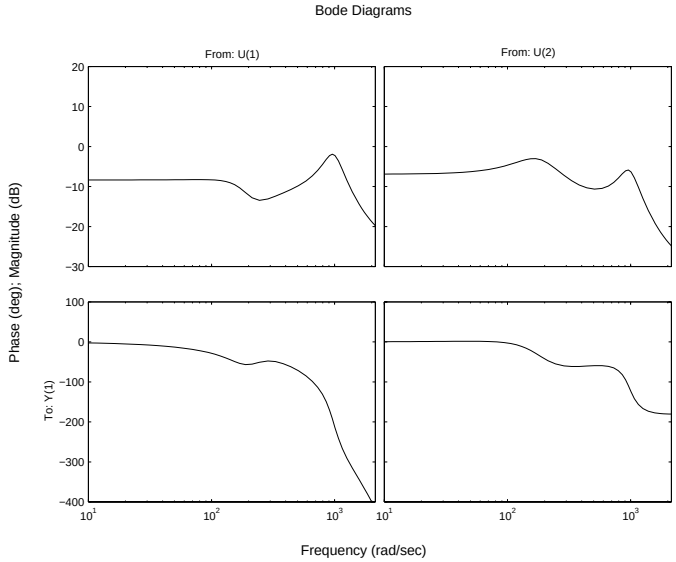

Figure 7.11 Bode diagram, Patient 1, AF. Output: 7th Pole, Inputs: 6th and 8th Poles, order=4.

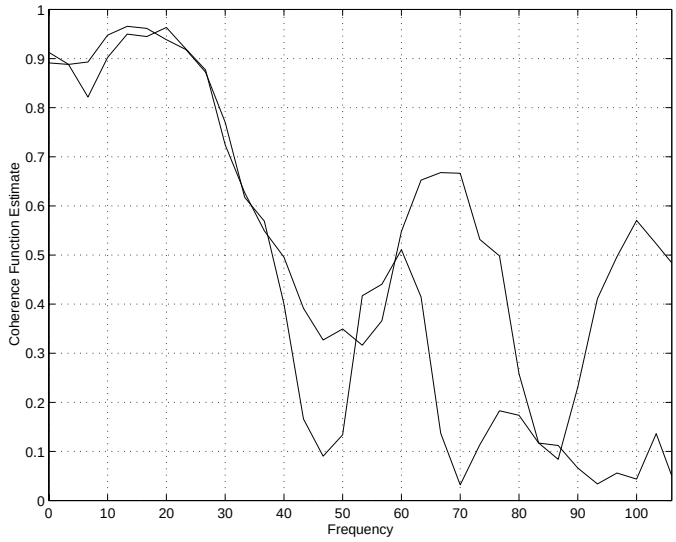

Figure 7.12 Coherence function, Patient 1, AF. Output: 7th Pole, Inputs: 6th and 8th Poles, order=4.

sions, which was infeasible at the moment of the study due to limitations in available catheters.

The validity of the method was enhanced looking into the results during sinus rhythm. The normal cardiac rhythm is initiated from sinus node, close to the entrance of the superior caval vein into the right atrium, then it propagates along the entire myocardium. The *direction and speed of excitation* obtained in our study confirmed the expectations from previous studies [7,13,14]. Furthermore, elevated maximum correlation coefficients, compared to those obtained during AF, showed high consistency in propagation, as it is known during sinus rhythm.

High accuracy in resulting models manifested *linear relation* among signals in the coronary sinus catheter. It was also confirmed by computing the

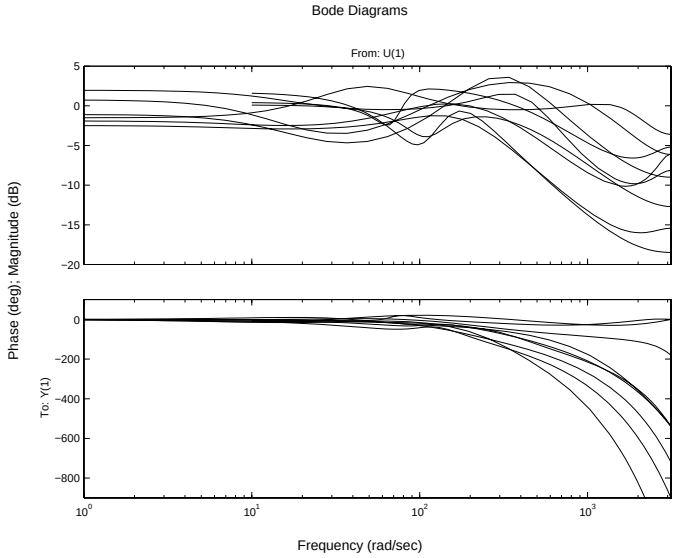

Figure 7.13 Bode diagram, Patient 7, SR, Output: Pole i-1, Input: Pole i, order=4.

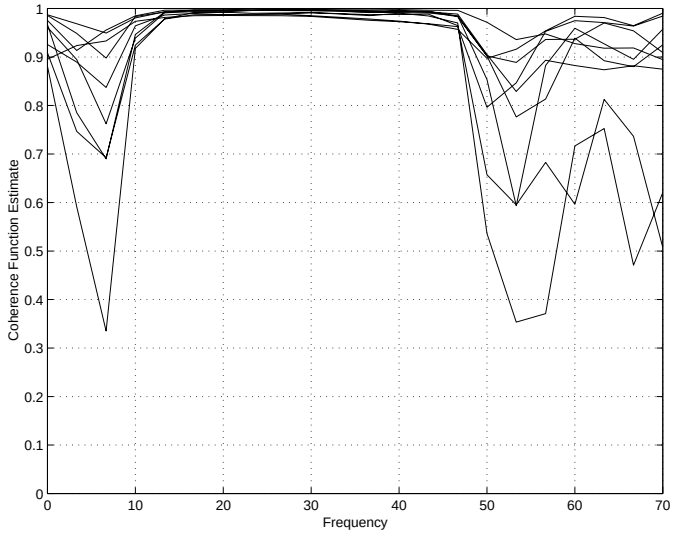

Figure 7.14 Coherence function, Patient 7, SR, Output: Pole i-1, Input: Pole i, order=4.

coherence function which presented values close to one for low frequencies (including the fibrillation frequency). In addition, cross validation simulation showed our system, electrical propagation among electrodes, was time invariant during intervals belonging to the same data set and patient. The manifested linear and *time invariant* relation among unipolar signals could stimulate future research in building models of electrical activity inside the heart during different basal rhythms.

Comparing the bode diagrams of each input-output system, similar characteristics can be observed. Furthermore, the phase diagram presents a decreasing slope while frequency increases which is due to the delay between input and output shown by the previous correlation analysis.

Substitution of the ventricle response in endocardial electrograms could be done using other methods. However, the linear interpolation between

the limits of QRS-complex in lead V1 surface-ECG has accomplished our purpose in terms of consistency in results. Future work could be done applying a different method to substitute the ventricular activation in the signals. Similar results in propagation direction and speed over signals treated with the new method would show congruity among methods.

7.11 Conclusions

Despite the fact that different wave front directions have been found, depending on the patient, we have demonstrated consistency in electrical activity propagation during atrial fibrillation along coronary sinus in all cases with only one exception. This could lead to future interpretations and work applying the same procedure on signals spread out inside the atria, ideally in three dimensions, where no ventricle response can distort atria activations for analysis. However, we have tested our procedure on signals during sinus rhythm obtaining the expected results in speed and direction of excitation as well as high consistency in patterns.

8. Final Conclusions

- It has been shown that correlation analysis is an efficient tool to study spatial and temporal propagation of atrial activity. Consistent patterns in propagation direction have been shown in five patients out of six during atrial fibrillation and in one during sinus rhythm. It could be also applied to other electrograms from different points in the heart to draw a picture of electrical propagation inside the heart during different basal rhythms.
- Linear relation among endocardial electrograms from coronary sinus and time invariant systems have been presented by computing simple linear models based on least squares method.
- We have applied an impulse response method to reproduce atrial activations during atrial fibrillation and during sinus rhythm in ten endocardial electrograms from coronary sinus simultaneously. In this case, there is no need of measuring the input which is considered to be an impulse generated in the sinus node. This method is only useful in local prediction of atrial activations but not for prediction in the long term.
- Finally, Subspace Model Identification (SMI) methods have been applied to show an input-output relation among signals from inside the heart (endocardial electrograms from coronary sinus) and signals from outside the heart (V1 Surface-ECG).

9. Bibliography

[1] G. K. Moe. On the multiple wavelet hypothesis of atrial fibrillation. *Arch Int. Pharmacodyn Ther*, 140:183–188, 1962.

[2] M. A. Allessie, W. J. E. P. Lammers, F. I. M. Bonke, and J. Hollen. Experimental evaluation of Moe's multiple wavelet hypothesis of atrial fibrillation. In D. P. Zipes and J. Jalife, editors, *Cardiac arrhythmias*, pages 265–275. Grune and Stratton, NY, 1985.

[3] K. T. S. Konings, C. J. H. J. Kirchhof, J. R. L. M. Smeets, H. J. J. Wellens, O. C. Penn, and M. A. Allessie. High-density mapping of electrically induced atrial fibrillation in humans. *Circulation*, 89(4):1665–1680, 1994.

[4] J. L. Cox, T. E. Canavan, R. B. Schuessler, M. E. Cain, B. D. Lindsay, C. Stone, P. K. Smith, P. B. Corr, and J. P. Boineau. The surgical treatment of atrial fibrillation II. Intraoperative electrophysiologic mapping and description of the electrophysiologic basis of atrial flutter and atrial fibrillation. *J. Thorac. Cardiovasc. Surg.*, 101:406–426, 1991.

[5] E. P. Gerstenfeld, A. V. Sahakian, and S. Swiryn. Evidence for transient linking of atrial excitation during atrial fibrillation in humans. *Circulation*, 86:375–382, 1992.

[6] M. Holm, R. Johansson, S. B. Olsson, J. Brandt, and C. Lührs. A new method for analysis of atrial activation during chronic atrial fibrillation in man. *IEEE Trans. Biomedical Engineering*, 43(2):198–210, February 1996.

[7] P.G. Platonov, S. Yuan, E. Hertervig, O.Kongstad, A. Roijer, A. B. Vygovsky, L.V. Chireikin, and S.B. Olsson. Further evidence of localized posterior interatrial conduction delay in lone paroxysmal atrial fibrillation. *Europace*, 3, January 2001.

[8] R. Johansson, M. Holm, S. B. Olsson, and J. Brandt. System identification of atrial activation during chronic atrial fibrillation in man. *IEEE Transactions on Automatic Control*, 43(6):790–799, June 1998 1998.

[9] M. Holm, R. Johansson, J. Brandt, C. Lührs, and S. B. Olsson. Epicardial right free wall mapping in chronic atrial fibrillation—documentation of repetitive activation with a focal spread—a hitherto unrecognized phenomenon in man. *European Heart Journal*, 18(2):290–310, February 1997.

[10] M. Holm, S. Pehrson, M. Ingemansson, L. Sörnmo, R. Johansson, L. Sandhall, M. Sunemark, B. Smideberg, C. Olsson, and S. B. Olsson. Noninvasive assessment of the atrial cycle length during atrial fibrillation in man: Introducing, validating and illustrating a new ECG method. *Cardiovascular Research*, 38:69–81, 1998.

[11] J. Carlson, R. Johansson, and S. B. Olsson. Classification of electrocardiographic P-wave morphology. In *IEEE Conf. Decision and Control (CDC 2000)*, Sydney,Australia, December 2000.

[12] P.G. Platonov, J. Carlson, M.P. Ingemansson, A. Roijer, A.Hansson, L.V. Chireikin, and S.B. Olsson. Detection of inter-atrial conduction defects with unfiltered signal-averaged P-wave ECG in patients with lone atrial fibrillation. *Europace*, 2:32–41, January 2000.

[13] F. Roithinger, J. Cheng, and A. SippensGroenewegen et al. Use of electroanatomic mapping to delineate transseptal atrial conduction in humans. *Circulation*, 100:1791–1797, 1999.

[14] M. Antz, K. Otomo, and M. Arruda et al. Electrical conduction between the right atrium and the left atrium via the musculature of the coronary sinus. *Circulation*, 98:1790–1795, 1998.

[15] D. S. Bayard. An algorithm for state-space frequency domain identification without windowing distortions. *IEEE Transactions Automatic Control*, 39(9):1880–1885, 1994.

[16] B. L. Ho and R. E. Kalman. Effective construction of linear state-variable models from input/output functions. *Regelungstechnik*, 14:545–548, 1966.

[17] J. N. Juang and R. S. Pappa. An eigensystem realization algorithm for modal parameter identification and model reduction. *Journal of Guidance, Control and Dynamics*, 8:620–627, 1985.

[18] M. Verhaegen and P. Dewilde. Subspace model identification—the output-error state-space model idenfication class of algorithms. *Int. J. Control*, 56:1187–1210, 1992.

[19] Haverkamp B. *Subspace Method Identification, theory and practice*. Department of Electrical Engineering, Delft, The Netherlands, 2000.

[20] S. Y. Kung. A new identification and model reduction algorithm via singular value decomposition. In *Proc. 12th Asilomar Conference on Circuits, Systems and Computers*, pages 705–714, Pacific Grove, CA, 1978.

[21] R. Johansson. *System Modeling and Identification*. Prentice Hall, Englewood Cliffs, NJ, 1993.

[22] J. N. Juang. *Applied System Identification*. Prentice Hall, Englewood Cliffs, NJ, 1994.